An analysis of three-dimensional patterns of experimental detonation cells

Vianney Monnier, Vincent Rodriguez, Pierre Vidal, Ratiba Zitoun

An analysis of three-dimensional patterns of experimental detonation cells

Vianney Monnier*, Vincent Rodriguez, Pierre Vidal, Ratiba Zitoun

Institut Pprime, UPR 3346 CNRS, Fluid, Thermal and Combustion Sciences Department, ENSMA, Téléport 2, 1 Av. Clément Ader, Chasseneuil-du-Poitou, 86360, France

Abstract

The notions of regularity and characteristic width of detonation cells are revisited based on crossed analyses of experimental front-view and longitudinal recordings obtained with the soot-plate technique. Tubes with cross-sections of different shapes, namely round, triangular and square, but the same surface area of 16 cm^2, are used to detonate the stable mixture $2\,H_2 + O_2 + 2\,Ar$ with the initial pressure p_0 varying from 15 kPa to 100 kPa and the initial temperature $T_0 = 294$ K. The longitudinal recordings show the well-known regular arrangements for this mixture for all cross-section shapes and p_0, but the front-view recordings show irregular patterns except for the square shape and low-enough p_0. There are fewer cells in the round tube, more in the square one, and their average widths and relative differences decrease with increasing p_0. All front-view cell patterns become irregular and independent of the cross-section shapes with increasing p_0. The cellular dynamics at the walls of a tube is thus not representative of that on the whole detonation front, and longitudinal soot traces alone are not sufficient for describing the cellular structure. An analysis based on graph theory proposes that a tessellation of regular hexagons can model a large set of irregular front-view cells. A cell count on an experimental front-view recording thus defines an average cell width and an intrinsic but high minimum error for this width. Its resulting large sensitivity to the parameters of a simple Arrhenius rate of chemical progress indicates that detailed schemes of chemical kinetics and more advanced conceptual tools than a single length are necessary for characterizing the three-dimensional structures of detonation cells. The Voronoi tessellation supplemented with a physical criterion for the surface density of randomly-distributed point sources could represent a step forward.

*Corresponding author: vianney.monnier@ensma.fr

1. Introduction

The instability of the reaction zones of self-sustained, e.g., Chapman-Jouguet (CJ), or overdriven detonation waves in gaseous mixtures was identified experimentally in the late 1950s by Denisov and Troshin [1], preceded by the observations of marginal detonations by Campbell and Woodhead [2]. Detonation fronts thus have a cellular structure, which is an impressive example of non-linearities in compressible reactive fluid dynamics such as those investigated by Clavin [3] for several varieties of reactive fronts. Higgins [4], Ng and Zhang [5], Vasil'ev [6], and Desbordes and Presles [7] reviewed experimental and numerical progress on detonation instability and cells. Understanding and characterizing this instability is useful for studying chemical kinetics in detonation reaction zones, calibrating numerical simulations and presizing safe industrial devices and advanced propulsion systems [8–10].

To date, the cellular structure of the detonation is characterized based on representative lengths, namely the average width of the cells [11], and the effective length of the reaction zone, that is, the Soloukhin's hydrodynamic thickness [12] further investigated by Lee and Radulescu [13, 14]. The increase in computational capabilities makes it possible to consider today predictable numerical simulations and other descriptions than characteristic lengths. This requires first collecting and analysing experimental data specific to the three-dimensional aspects of detonation cells, which is the object of this work.

The reaction zone of detonation in gases is an unsteady three-dimensional flow with unburnt and burnt gas pockets, and preceded by a leading shock made up of cells, that is, Mach waves with longitudinal and transverse fronts. Mach's method of traces on soot-coated plates is the usual technique to record geometrical information about cellular structure, [1, 15]. The typical setup is a straight detonation tube with the coated plates positioned longitudinally against its inner walls. The transverse waves erode the coating, which draws the diamond-shaped patterns that usually identify the detonation cells. Generally, their average widths and regularity [16, 17] depend on the equivalence ratio, dilution, initial pressure and temperature of the mixture [18–21], and on its confinement, such as a straight or a curved channel. They also depend on the wavefront dynamics, such as steady propagation in a tube, transmission from a tube to a large volume, or spherical expansion after direct ignition from a point source. The reference width is obtained with fronts travelling at the CJ velocity in a straight tube and is the length most often used for characterizing the cellular structure. It is defined as the average of the largest distances between the tracks of two contiguous transverse waves travelling in opposite directions (Subsect. 3.1). Values are available for many reactive mixtures [22].

The average width is accepted as a detonability indicator, that is, the capability of detonation to propagate in a system with finite transverse dimensions (another is the distance for the transition of deflagration to detonation, DDT). Thus, the smaller this width (or the DDT distance), the higher the detonability [23]. Shepherd et al. [24] and Zhao et al. [25] proposed automated methods to quantify cell width and irregularity using spectral and statistical analyses, respectively. More recently, Zhang et al. [26] reconstructed the cellular surface using the neural approach.

Cellular patterns on longitudinal soot foils have been categorized as very regular, regular, irregular and very irregular [16, 27], based essentially on recordings in square-section tubes. The average width of irregular patterns can thus be as large or even smaller than standard deviation, raising questions on its representativeness [17]. Cell regularity is interpreted based on the chemical kinetics in the detonation reaction zone [28–34]. Regular patterns are observed in mixtures with light fuels and oxygen highly diluted by a mono-atomic inert gas, typically argon, and irregular patterns in mixtures with heavier fuels and dilution with nitrogen [7]. Mixtures with regular or irregular patterns are also termed stable or unstable, respectively [25, 35, 36]. Short [37] and Radulescu [38] carried out a modelling synthesis based on the Zel'dovich-Neuman-Döring (ZND) model of the detonation reaction zone. Irregularity corresponds with ZND induction zones large compared to reaction thicknesses. They proposed a regularity criterion based on the ratio of the former to the latter (the χ number), the larger this ratio, the more unstable (irregular) the mixture. These interpretations thus involves chemical kinetics alone, whereas the shape of the cross-section of the detonation tube also determines how detonation cells behave. For example, regular mixtures show rectangular front-view cellular patterns only in tubes with rectangular cross-section, [39], and the marginal regimes of detonation propagation in regular mixtures are different depending on the cross-section shape. The usual control parameter for selecting marginal or multi-cellular detonation regimes in a given tube is the initial pressure because the larger it is, the smaller the cells.

There are only a few cells on the front of marginal detonations, and only one for the lower limit of propagation [2, 40, 41]. For the round cross-section, the limiting mode shows a spinning wave, that is, a single transverse wave rotating along the tube wall [42–45]. For the square cross-section, the limiting mode shows two transverse waves normal to each other and reflecting on facing walls [42]. For slightly larger initial pressures, there can be two pairs of parallel transverse waves, each pair normal to the other and each wave of the same pair moving in opposite directions. The usual observation is the rectangular mode for which the transverse waves of a same pair are parallel to facing walls [46]. However, Hanana et al. [39, 47] identified a diagonal mode for which the transverse waves are angled by $\pi/4$ to the tube walls, by passing the detonation through an obstacle with a square hole angled by $\pi/4$ to the walls. Inductively, these experiments indicate that the three-dimensional properties of a cellular structure in a given mixture at given initial pressure and temperature depend on the dimension and the shape of the confinement [48] and, for marginal regimes, on the ignition method. Williams et al. [49] carried out first 3D numerical simulations of the two one-cell rectangular modes, thus anteceding the experimental observations by Hanana et al. [39, 47]. They described these modes as a pair of superimposed 2D ones, and identified, in particular, the phase shift issue. They also compared 2D and 3D numerical simulations and found the same cell width regardless of the dimensionality. Deledicque et al. [50] and Dou et al.[51] reached the same conclusion. Most numerical simulations of rectangular and diagonal modes are based on inviscid (Euler) equations coupled to detailed chemical-kinetics schemes or simple Arrhenius rates combined with the constant-γ equation of state, [52–57].

The converse situation is that of cells small compared to the transverse dimensions of the tube or to the detonation size itself such as the radius of a spherically expanding detonation. Although there are many observations and recordings of multi-cellular regimes of detonation, the geometrical properties of a large set of cells seem to have received less attention, apart from the indication by Takai et al. [58] that the volumes drawn by the transverse waves of rectangular modes are octahedrons and tetrahedrons. Therefore, recording implementations aiming at the 3D reconstruction of the cells should also investigate how the structure of multi-cellular fronts depends on the geometrical properties of the confinement, as suggested by Presles et al. [59].

Our work thus describes and analyses experiments in tubes whose cross-sections have different shapes, namely square, triangular and cylindrical, based on front-view and longitudinal cell recordings on soot-coated foils for the regular mixture $2\,H_2 + O_2 + 2\,Ar$. This study is essentially experimental and descriptive, and intended only to discuss the cellular patterns, not to provide a predicting model for their sizes. Section 2 details the setups and their instrumentation, Section 3 presents the experimental results, Section 4 investigates how elements of graph theory can help interpret these results, and Section 5 discusses and concludes the work.

2. Experimental methodology and setup

We carried out a series of recordings in tubes with round (R), equilateral triangular (T) and square (Q) cross-sections of the same area 16 cm^2 to within ± 4 % . We also carried out some in round and square tubes with larger areas (R' and Q' resp.). Table 1 shows the inner dimensions of the tubes; Figure 1 shows the schematic of a round or square tube. The T tube was 1 m long; it was inserted in the 10 m long R' tube at its end opposite ignition. A spark plug or an exploding wire was used for ignition, Shchelkin spirals then ensured the transition to detonation on a very short distance, typically 1 m.

We selected the stoichiometric reactive mixture $2\,H_2 + O_2 + 2\,Ar$ because its regular cellular pattern in square tubes at low-enough initial pressures (Section 1) is a convenient reference for comparison with the patterns in the round and triangular tubes. The mixture was prepared in a separate tank using the partial-pressure method, and then injected at the desired initial pressure p_0 after vacuuming the tubes. We varied the initial pressure p_0 from 15 kPa to 100 kPa and the initial temperature was 294 ± 3 K for all experiments.

Tube	Cross-section area (cm^2)	Diameter or side length (mm)	Length (m)
R	16.6	46	6
T	16.1	61	1
Q	16.0	40	6
R'	70.8	95	10
Q'	25.0	50	6

Table 1: Dimensions of the tubes. R, R': round, T: equilateral triangle, Q, Q': square

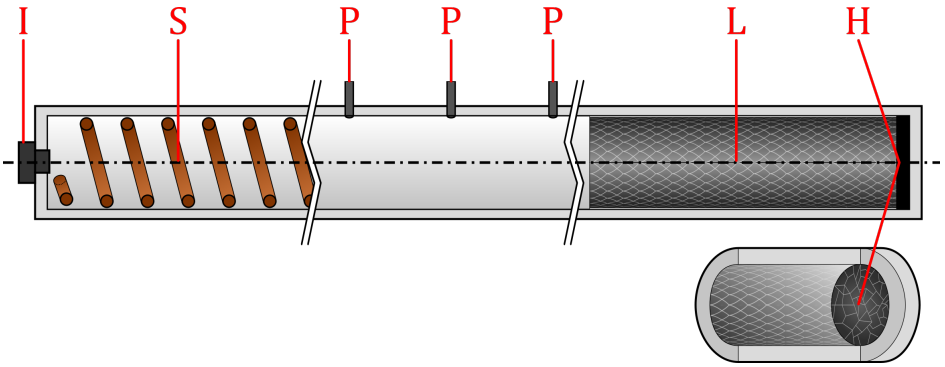

Figure 1: Schematic of a round or square tube.
I: ignition, S: Shchelkin spiral, P: pressure transducers, L: longitudinal soot foil, H: end-on soot foil

We recorded the longitudinal and front views of the cellular structure on soot-coated foils. We obtained the front views using the basic method of the head-on impact of the detonation front with the foil positioned normal to the cross-section at the tube end [1, 60]. We found it easier to implement than the optical method [59], originally devised for liquids, of the head-on impact with an illuminated aluminized foil (the cellular-front imprint deflects the light in different directions, and a synchronized camera records the foil deformation at the instant of the impact, hence the cells). We positioned the foils for the longitudinal recordings in the round and square tubes against their inner walls, at their ends opposite ignition. They were shaped into a half-cylinder for the round tubes and a plate for the square tubes, with length and thickness 50 cm and 1 mm, respectively. The three inner faces of the T tube were coated over their whole length (1 m) before being assembled in such a way as to ensure sharp and equal inner angles.

Three Kistler 603B pressure transducers coupled to Kistler 5018A electrostatic charge amplifiers were positioned on the round and square tubes before their soot-foil section. We used the triggering of the transducers to obtain the average velocity of the detonation wave and check its steadiness in the soot-foil section.

We also checked steadiness from the longitudinal recordings with the criterion that cells should have average geometrical properties constant from the beginning to the end of the soot foil. We could not position transducers on the T tube, and we checked steadiness, in this case, from the soot recordings solely. We always observed constant average geometrical properties along the total lengths of the square and round tubes and from about 10 cm from the entry of the 1 m long T tube.

3. Results

3.1. Cell patterns and cross-section shapes and areas

Figures 2 to 5 show typical front-view and longitudinal soot recordings.

At lower initial pressures, from $p_0 = 15.0$ to 20.0 kPa (Figures 2 to 4, respectively), the front-view recordings in the Q tube show the long-time identified regular arrangement of

square and rectangular patterns whose distributions depend on the instant of the detonation impact. These distributions are analyzed in subsection 3.2. However, the arrangements in the T and R tubes are stochastic, and repeated experiments show no dependence on the instant of impact. Although counting is difficult, a detonation front in an R tube appears to contain fewer cells than in the T and Q tubes, and in the T tube than in the Q tube, for the same p_0. The longitudinal soot recordings shows cells more irregular in the T and R tubes than in the Q tube. They also show cells longitudinally slimmer in the Q tube than in the T and R tubes, that is, the cell length (L) to width (λ) aspect ratios in the R and T tubes are closer to unity. In the Q tube, they also show a regular spacing of the reflection impacts of the transverse fronts moving parallel to the longitudinal plate.

At intermediate initial pressures, from 20.0 to 70.0 kPa (Figures 5 and 6, respectively), the rectangular patterns on the front-view recordings in the Q tube are locally deformed with complex shapes similar to those on the T and R front-view recordings. The deformation domains have a stochastic distribution and spread with increasing p_0, although the longitudinal recordings in the Q tube still show a regular spacing of the transverse impacts.

At higher initial pressures, from $p_0 \approx 70.0$ kPa (Fig. 6), the deformation domains eventually cover the whole section of the Q tube. There is no transverse waves moving parallel to the walls and no impacts of transverse fronts on the longitudinal plate anymore. The front-view patterns look the same regardless of the cross-section shape. They show the same complexity without evident local and global symmetries. The longitudinal recordings in the Q tube (Fig. 6) also look the same as in the T and R tubes, in particular, they do not show reflection impacts of the transverse fronts anymore, as they did for the lower and intermediate p_0.

The longitudinal soot recordings point to two other observations. The first is the paradoxical result that the longitudinal patterns are regular even in the cases where the front-view patterns are not, regardless of the tube. The second is that the cells are slimmer in the Q tube than in the T and R tubes. Although perhaps limited to regular mixtures, this opposite evolution participates in raising questions about the representativeness conditions of a single length for characterizing detonation cells, at least about those deduced from longitudinal recordings alone.

Nevertheless, Figure 7 shows the cell average widths λ from longitudinal recordings for each cross-section shape as function of the initial pressure p_0. The widths were defined classically as the largest distances between two transverse waves projected normal to the average incident shock direction [25, 29]. Their averaging includes at least 50 measurements along each recording, and the resulting uncertainty is approximately the size of the coordinate markers in the figure. These averages show the usual decreasing trend with increasing p_0 regardless of the cross-section shape and, if $p_0 > 25.0 - 30$ kPa, they meet the well-known empirical relation $\lambda \propto p_0^{-\alpha}$ with $1.1 < \alpha < 1.3$ [61]. Their differences from one shape to another increase with decreasing p_0. The difference from the Q to the R shapes increases progressively with p_0 decreasing from 20.0 kPa whereas that from the T to the R shape is more abrupt at p_0 about 15.0 kPa. The cell widths in the R tube are the larger, those in the Q tube the smaller. Their differences can be as large as $\sim 100\%$ for the lower initial pressure

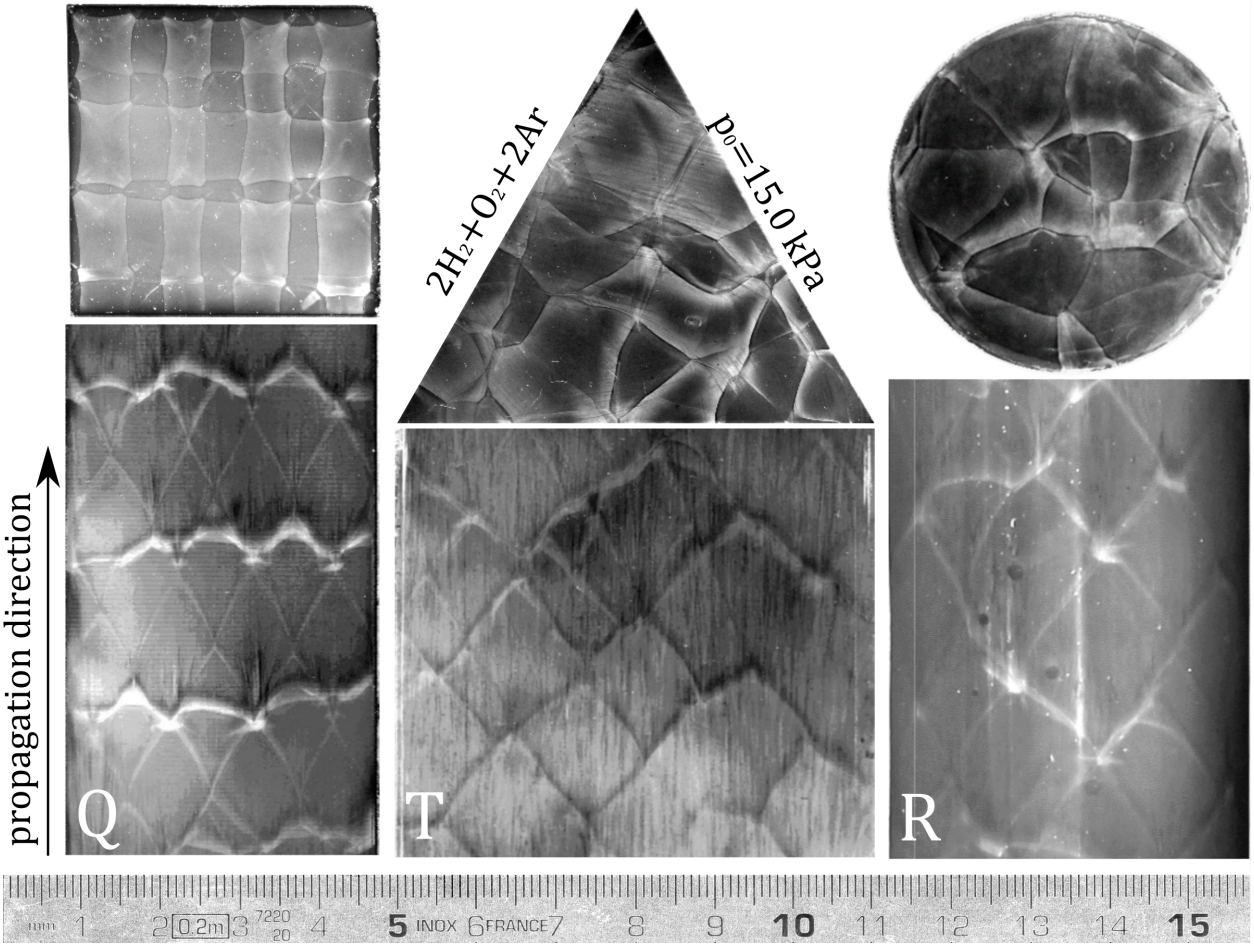

Figure 2: Front-view (top) and longitudinal (bottom) soot recordings in the mixture $2\,H_2 + O_2 + 2\,Ar$ at $p_0 = 15.0$ kPa in round (R), triangular (T) and square (Q) tubes with the same cross-section area (16 cm^2).

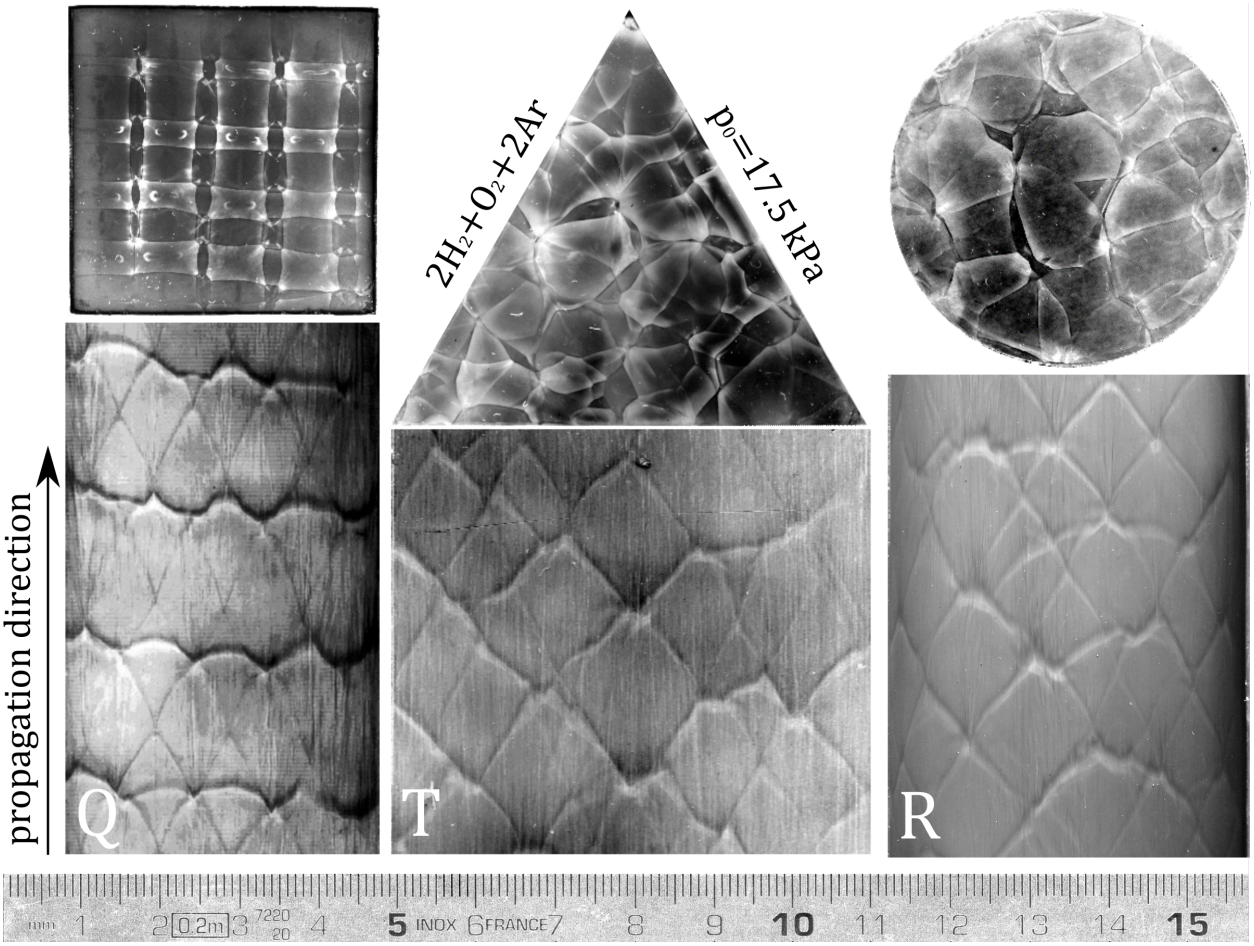

Figure 3: Front-view (top) and longitudinal (bottom) soot recordings in the mixture $2\,H_2 + O_2 + 2\,Ar$ at $p_0 = 17.5$ kPa in round (R), triangular (T) and square (Q) tubes with the same cross-section area (16 cm^2).

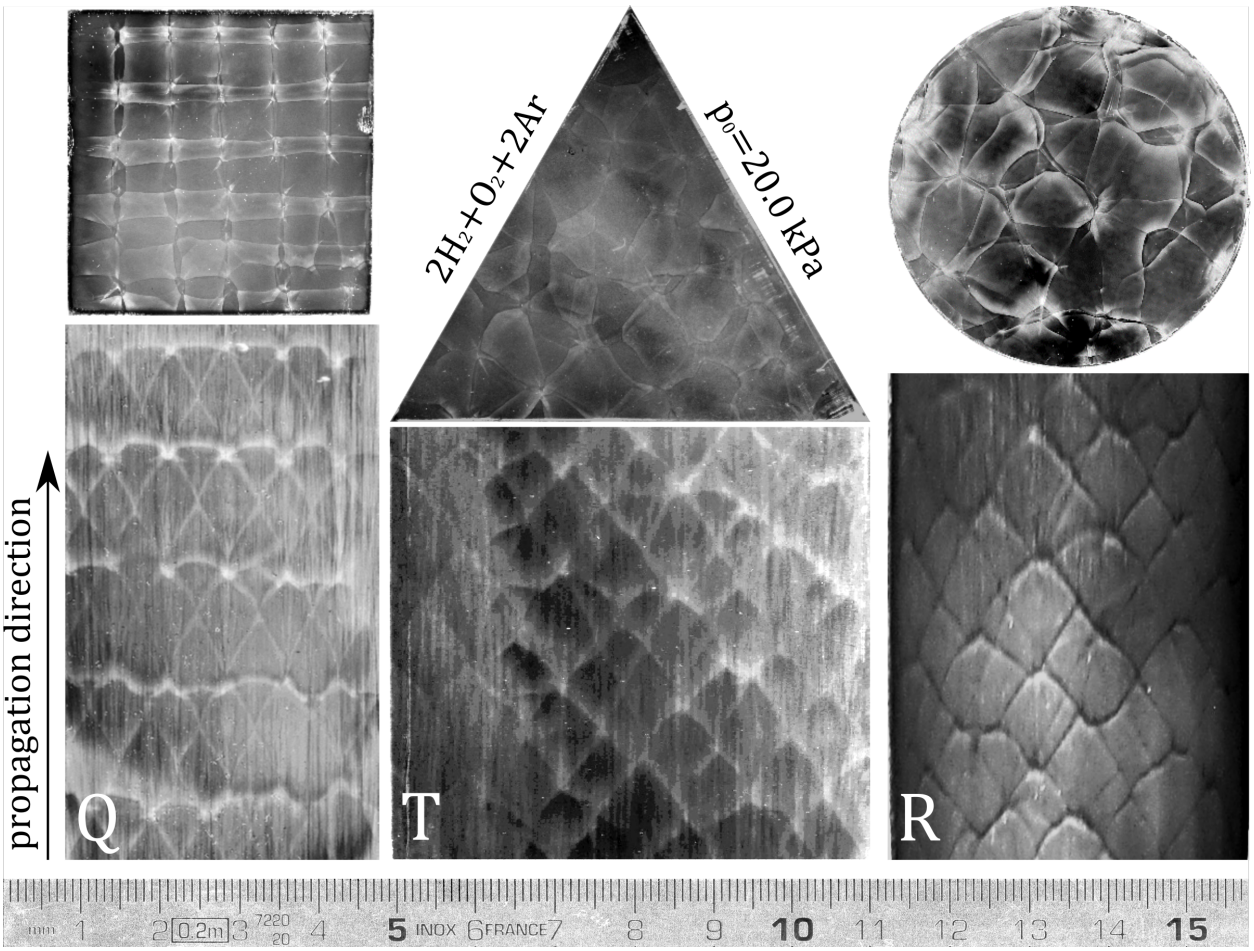

Figure 4: front-view (top) and longitudinal (bottom) soot recordings in the mixture $2\,H_2 + O_2 + 2\,Ar$ at $p_0 = 20.0$ kPa in round (R), triangular (T) and square (Q) tubes with the same cross-section area (16 cm^2).

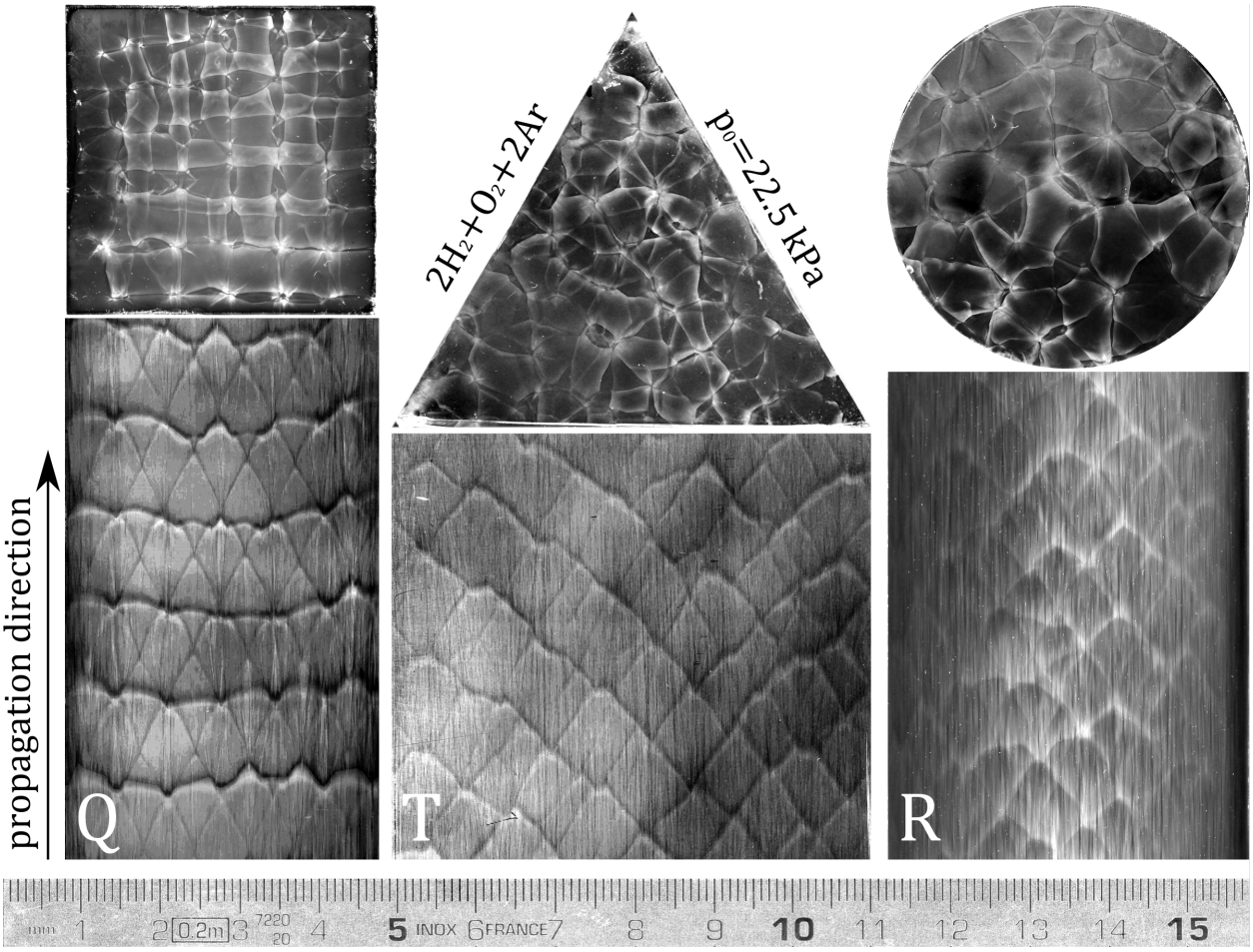

Figure 5: Front-view (top) and longitudinal (bottom) soot recordings in the mixture $2\,H_2 + O_2 + 2\,Ar$ at $p_0 = 22.5$ kPa in round (R), triangular (T) and square (Q) tubes with the same cross-section area (16 cm^2).

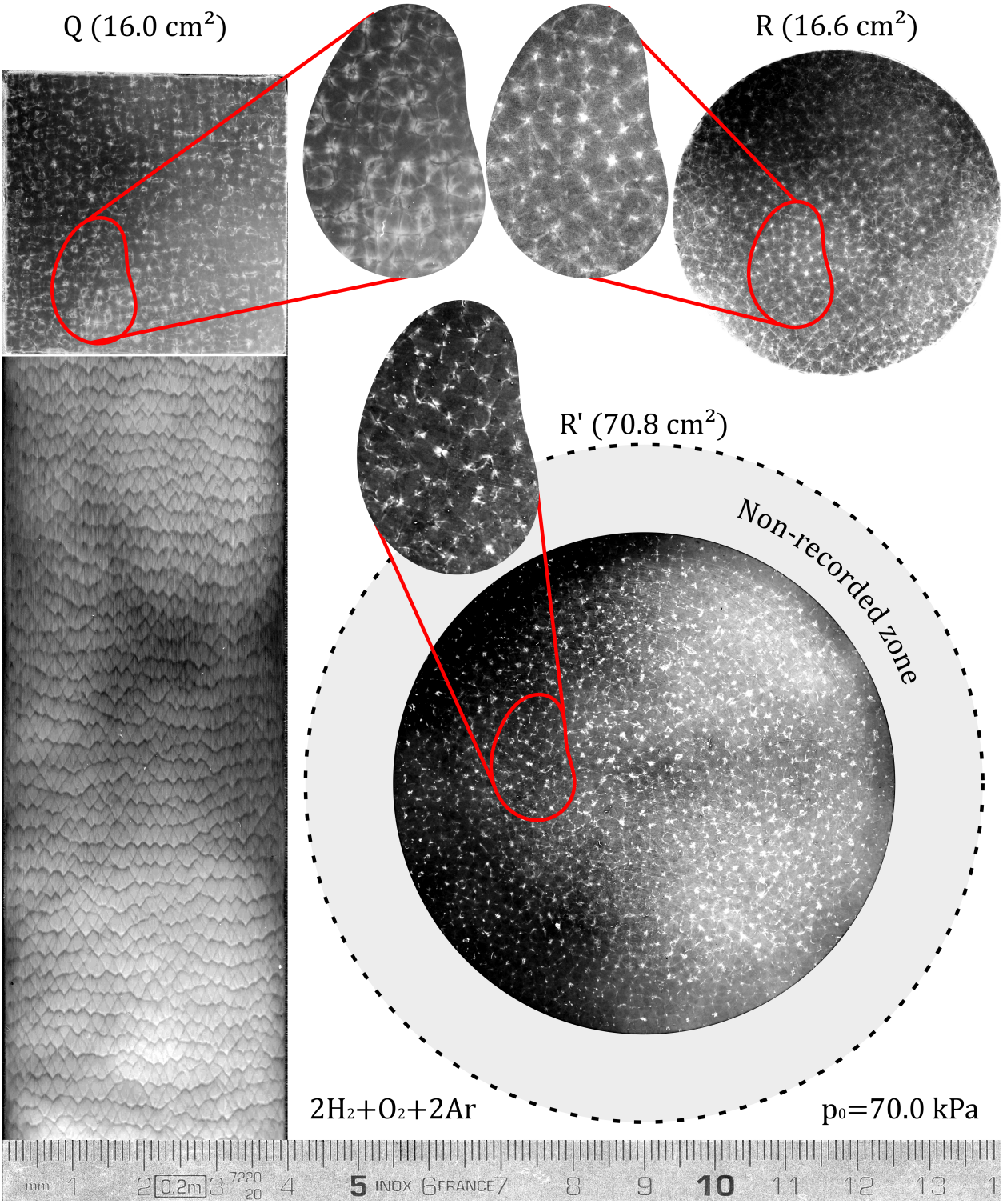

Figure 6: Front-view soot recordings in the mixture $2\,H_2 + O_2 + 2\,Ar$ in the Q, R and R' tubes and longitudinal soot recording in the Q tube at $p_0 = 70.0$ kPa. The periphery of the R'-tube cross-section could not be recorded.

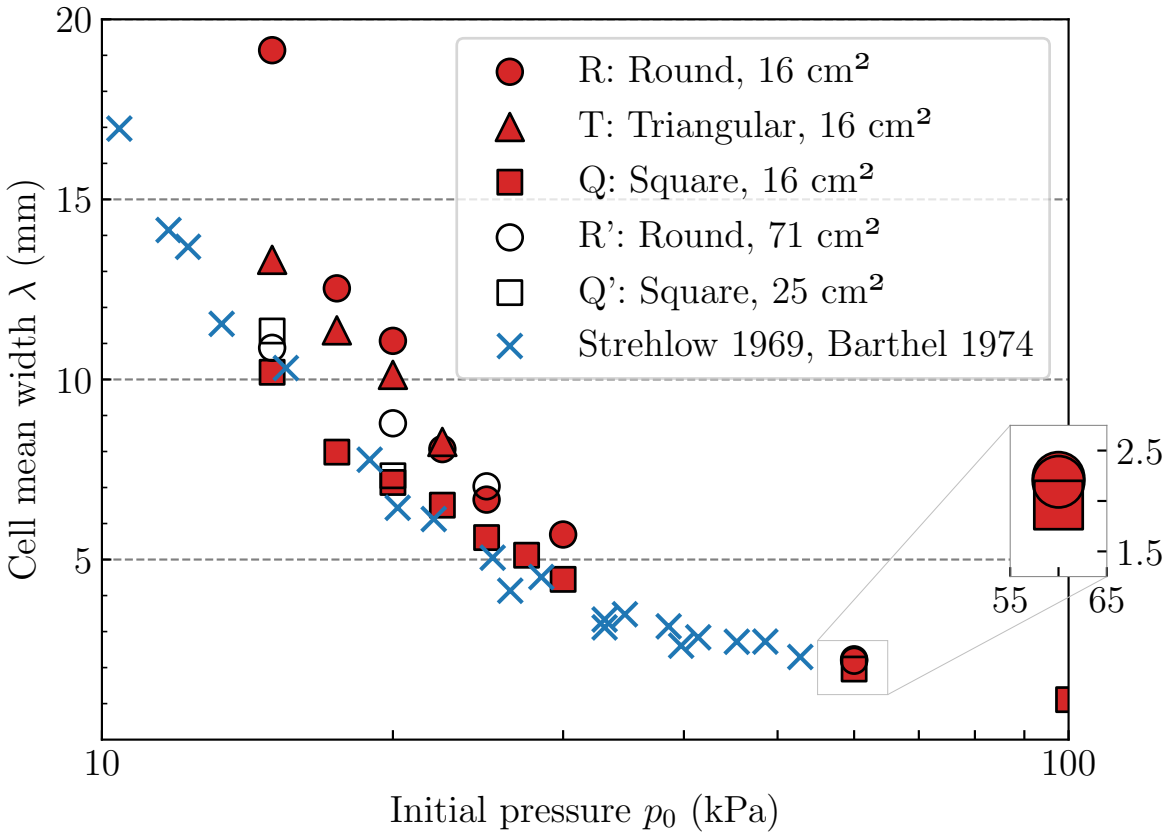

Figure 7: Cell average widths measured on the longitudinal soot recordings as function of the initial pressure p_0 and the shape and the area of the cross-section of the tubes.
Measurement uncertainty is about the same as the marker heights.

$p_0 = 15$ kPa. For a given p_0, the differences are small for the tubes whose cross-sections have the same shape and different areas.

There are two possible interpretations. The first is that no symmetry can result in the long term from the necessarily complex oblique reflections of transverse waves on round and triangular tube walls. The second is a boundary layer at walls. A variation analysis in the limit of large cross-sections appears not to favor the latter. For example, the basic Fay model [62, 63] reproduces at least qualitatively the increase of the boundary-layer thickness with decreasing p_0. The lower flow velocity due to viscosity in a boundary layer acts as a mass sink that induces locally a specific mass larger than in the entire cross-section. The consequences are a diverging flow and, therefore, a curvature and a velocity deficit of the average front [64–66], that should increase with increasing thickness of the boundary layer. This description applies to cellular detonations if the cell widths are small enough compared to the transverse dimensions of the tubes so that a smooth average surface represents well the detonation front. According to Figure 7, this effect should then be more pronounced in the R tube than in the Q tube since detonation cells are larger if the shock temperature, that is, the detonation velocity, is smaller. In the limit of large cross-sections, the boundary-layer thickness, denoted below δ, should be independent of the cross-section shapes and thin compared to the transverse dimensions of the tubes, namely here the radius R of the round tube and the side a of the square tube. Their cross-section areas are $A_R = \pi R^2$ and $A_Q = a^2$, those reduced by the cross-section areas of the boundary layers are $A'_R = \pi R^2(1-\delta/R)^2$ and $A'_Q = a^2(1-2\delta/a)^2$, so, since $A_R = A_Q$ in this work,

$$\frac{A'_Q}{A'_R} = \left(\frac{1-2\varepsilon}{1-\sqrt{\pi}\varepsilon}\right)^2, \tag{1}$$

with $\varepsilon = \delta/a$. This ratio is smaller than 1 for physically-small δ/a, and decreases with increasing δ/a. The effective cross-section area would thus be larger in a R tube than in a Q tube with the same geometrical cross-section area and would decrease less rapidly in an R tube than in a Q tube. Figure 7 shows the opposite trends, that is, the cell width is larger in the R tube than in the Q tube, and the difference increases with decreasing p_0. This observation suggest that, in our conditions, possible boundary layers have a characteristic time of development larger than that of chemical-kinetics termination, which tends to favor the hypothesis of asymmetry from complex oblique transverse reflections. Indeed, cells are still small compared to the transverse dimensions of the tubes. For example, $0.05 \leq \lambda/a \leq 0.2$ ($a = 40$ mm, Table 1) for $p_0 \in [70, 20]$ kPa approximately, a domain where an influence of the cross-section shapes is already observed. Another argument for the complex interplay of the transverse waves and the tube walls is that cells are slimmer in the Q tube than in the R and T tubes at lower p_0, but all attain the same aspect ratio with increasing p_0 regardless of the cross-section shape. The limiting initial pressures above which the λ values become independent of the cross-section shapes and the front-view patterns in the Q tube irregular appear to be approximately the same. We estimate this limiting p_0 to 70.0 kPa. However, although their cross-section areas are different (Table 1), the Q and Q' square tubes give similar cell widths even for the lower initial pressures. These widths agree well with those

reported by Barthel [67] and Strehlow [29] (also in [68]). Below $p_0 \leq 22.5$ kPa, the cell mean widths for the tubes with greater cross-section area (Q' and R', areas 25 and 70.8 cm^2, resp.) are smaller than in the T and R tubes (area 16 cm^2).

It has long been known that the transverse dimension of the tube affects the cellular and propagation dynamics of the detonation, all the more so as there are fewer cells on the front, depending on the initial pressure or temperature. Conversely, the smaller the cells, the more independent of the tube they are and the greater the contribution of chemical kinetics [69], p.194. For example, the increasing divergence of λ with decreasing p_0 was noted by Strehlow and Engel [29] when they compared their measurements to those of Voitsekhovskii [45], but we could not find the tube dimensions for these experiments. Similarly, Kumar and Dewit [70, 71] noted the increasing difference between their measured and theoretical cell widths with decreasing p_0. They invoked both measurement issues and the influence of the tube size because their modelling involved only the post-shock velocity and specific-heat ratio, the initial temperature, and the induction time.

Essentially, our experiments also point out the increasing influence of the cross-section shape with decreasing initial pressure, that is, with increasing cell widths. They also point out the difficulty to determine which minimum pressures ensure cell properties independent of the tube geometrical properties, that is, dependent on chemical kinetics alone.

3.2. Cells patterns and phase shift in square tubes

We carried out a detailed analysis of the detonation propagation in square-section tubes with p_0 low enough so there are transverse waves moving approximately parallel to the tube walls (Subsect. 3.1). We used the grey levels on the front-view recordings to infer the propagation direction of the transverse waves, which is from the lighter to the darker domains because the latter are made up of the soot particles not swept yet by these waves (Figure 8). We thus identified a continuum of rectangular modes of propagation (Section 1). Figure 9 shows a schematic, the coordinates x and y denote the transverse directions, and z the longitudinal one, i.e., that of the detonation propagation. A single longitudinal soot recording identifies the two sets of transverse waves defining a rectangular mode, one by the diamond-shaped patterns, the other by the periodic impacts of the transverse fronts moving about parallel to the soot plate.

It is convenient to introduce a phase shift φ defined as the distance between the longitudinal positions of the transverse-wave impacts in the x and y directions as schematized in Figure 9. Its minimum and maximum values are 0 and half a cell length $\varphi_{max} = L/2$, respectively, and the value used in Figure 9 is intermediate. This definition generalizes to multi-cellular regimes that identified numerically by Williams et al. [49] and experimentally by Hanana et al. [39] with one-cell marginal regimes (Section 1). For $\varphi = 0$, the two sets of transverse waves are in phase, with impacts at adjacent tube walls at the same position z (Figure 10, impact position z_2). The diagonals and the normals to the walls through the centre of the cross-section are symmetry lines of the cellular front regardless of time. Each cell has a fixed center and alternates a square and a rectangular shape, which periodically grows and shrinks with an aspect ratio oscillating between 0 and $+\infty$.

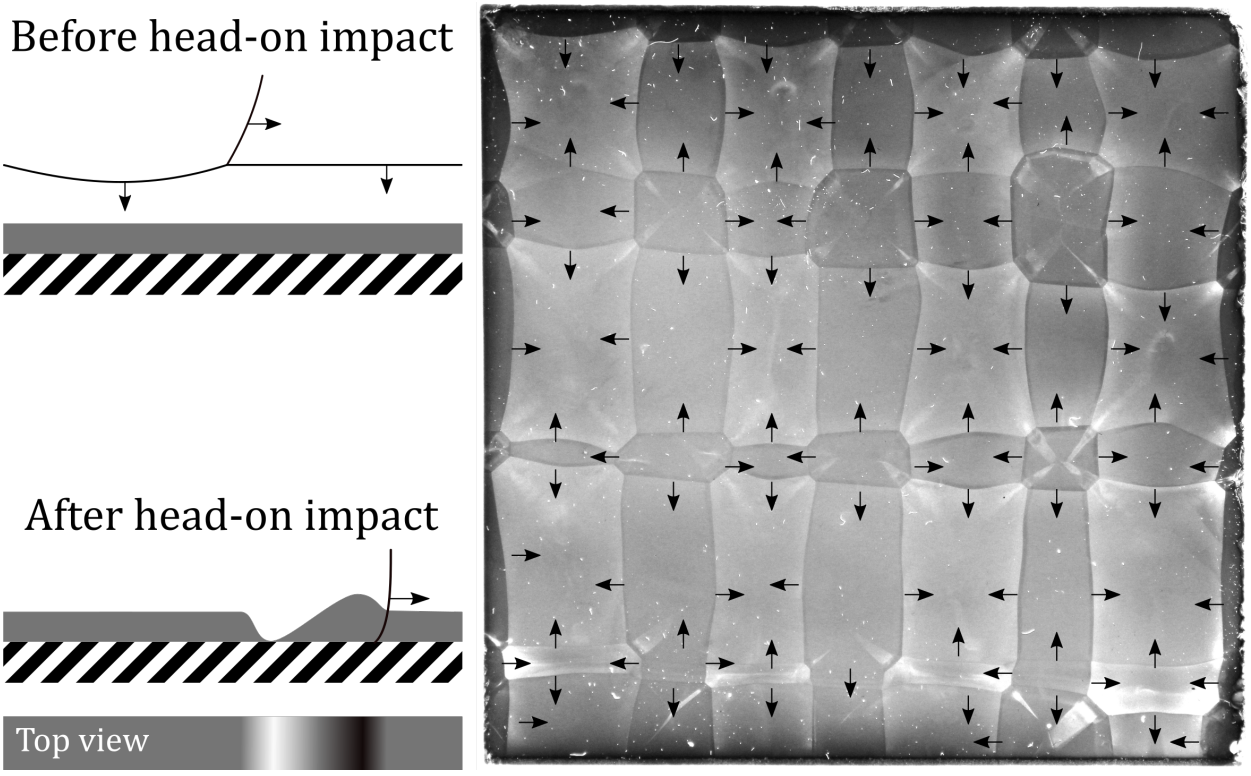

Figure 8: Left: side- and top-view schematics of the soot layer before (top) and after (bottom) the head-on impact. Right: head-on recording with the transverse-wave directions indicated by white arrow (mixture: $H_2 + \frac{1}{2}\,O_2 + Ar$, $p_0 = 15.0$ kPa, tube width $a = 40$ mm)

The opposite case corresponds to transverse sets in phase opposition. The phase shift φ reaches its maximum value $\varphi_{max} = L/2$ (Figure 11). Similarly to the in-phase case, the cell centers have fixed positions and the square and rectangle head-on shapes alternate between each other. There is no symmetry lines any more but the head-on structure looks as though it rotates by $\pi/2$ every time interval necessary for a longitudinal propagation be equal to $L/2$. In Figure 11, this corresponds to the positions z_1 and z_3, and z_2 and z_4.

In our conditions, each longitudinal recording showed a continuous variation of the phase shift φ between its minimum 0 and maximum $L/2$ Fig. 13, so the front-view recordings most often showed out-of-phase modes. Our interpretation is that the detonation propagation is also subjected to long-wavelength and low-amplitude instabilities - compared to the cell dynamics - that distort the average front so its surface is warped, hence the evolutive mode of the rectangular dynamics. This variation might result from an intrinsic instability of the rectangular mode growing with increasing cell number, that is, p_0, and from the system and ignition imperfections, such as small defects at the tube wall and an asymmetrical shape of the wave front that comes out of the Shchelkin spiral. Thus, the phase and its shift are difficult to identify and measure with a practical accuracy, and appear as concepts restricted to ideal ignition system, tube and cellular detonation front, that is, neither tilted, curved, nor warped.

Another observation is that the blowup of the crossing locus of two transverse waves reveals that each splits into the same third one, although they look about normal to each other (Figure 12, red and blue lines). Each propagates partly behind, partly ahead of the other, that is, on different initial states. Therefore, their front velocities are different, which requires a third wave for their matching (green line). Regular cells in square cross-section tubes are thus bounded by two incident shocks and two Mach stems (Figure 12, states (0) and (2), resp.), so they are octagons and not rectangles. More generally, four-wave crossings on a head-on recording appear to be fortuitous with a lifetime negligible compared to the evolution time of a detonation cell.

Our analysis here points out that long-time scales phenomena affect the regularity and the symmetry of detonation cells. Numerical simulations should thus consider investigating the propagation of cellular detonation based on initial and boundary conditions with stochastic distributions of imperfections representative of actual devices. Also, capturing the details of the transverse wave dynamics necessitates three-dimensional calculations, but whether these details significantly influences the overall detonation dynamics is an open debate.

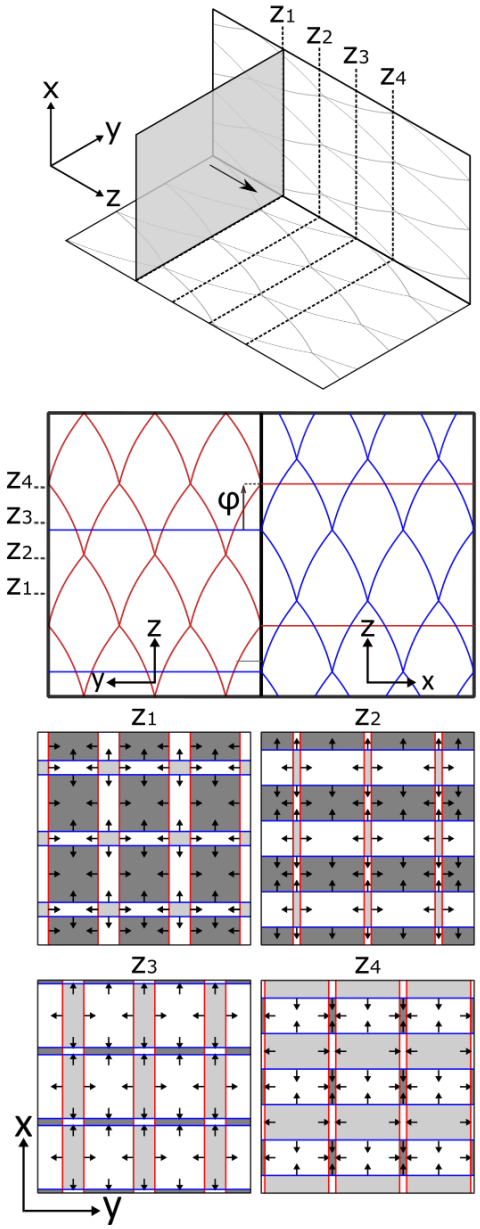

Figure 9: Schematics of the detonation cell evolution with an arbitrary phase shift $0 < \varphi < \varphi_{max}$

.

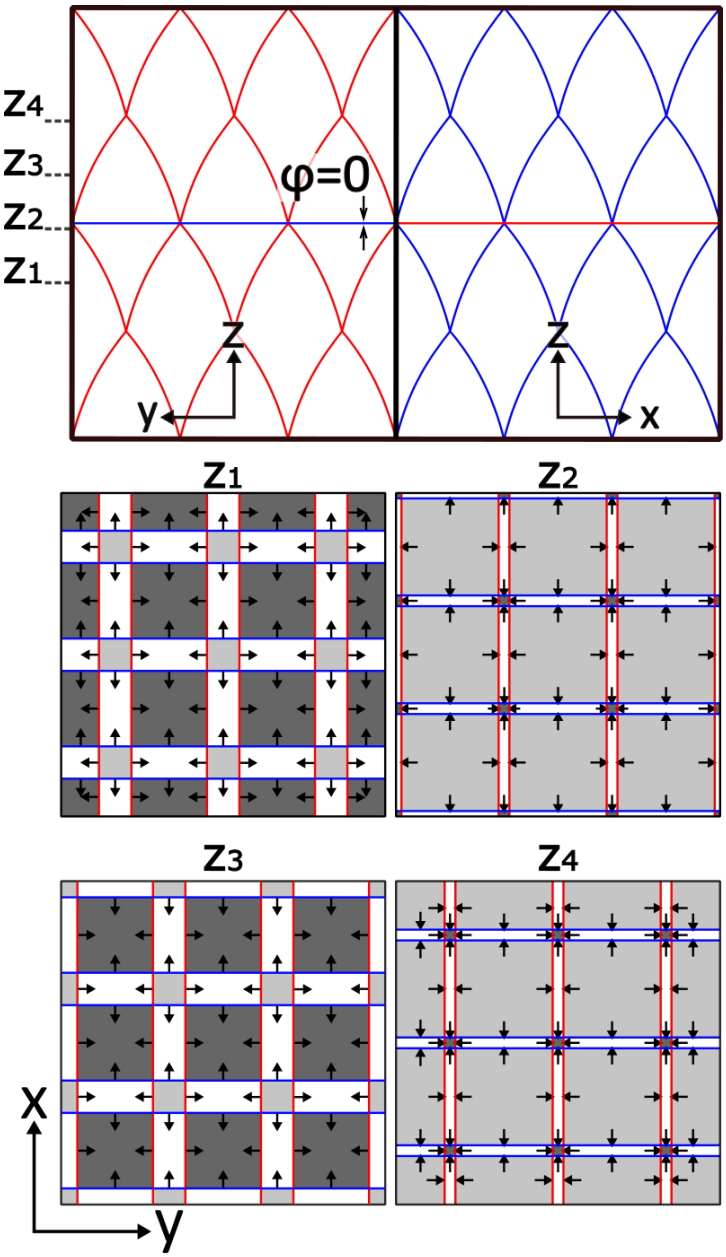

Figure 10: Schematics of the detonation cell evolution with minimum phase shift $\varphi = 0$

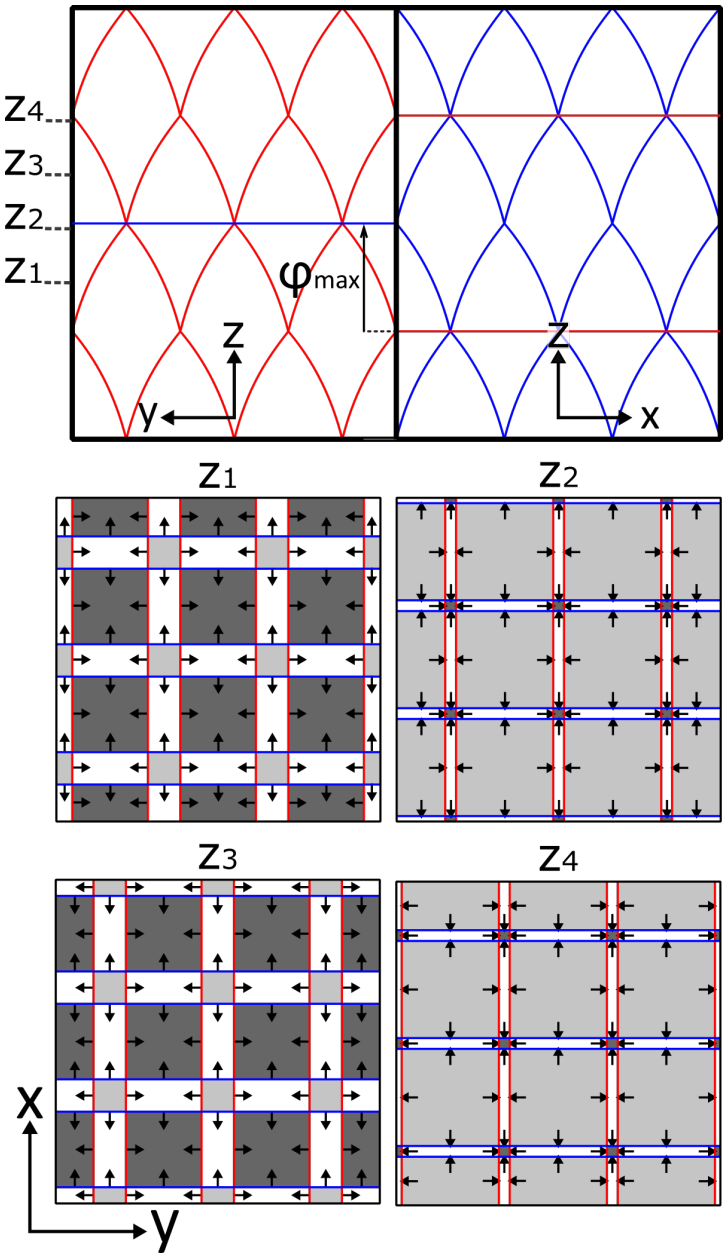

Figure 11: Schematics of the detonation cell evolution with maximum phase shift $\varphi_{max} = L/2$

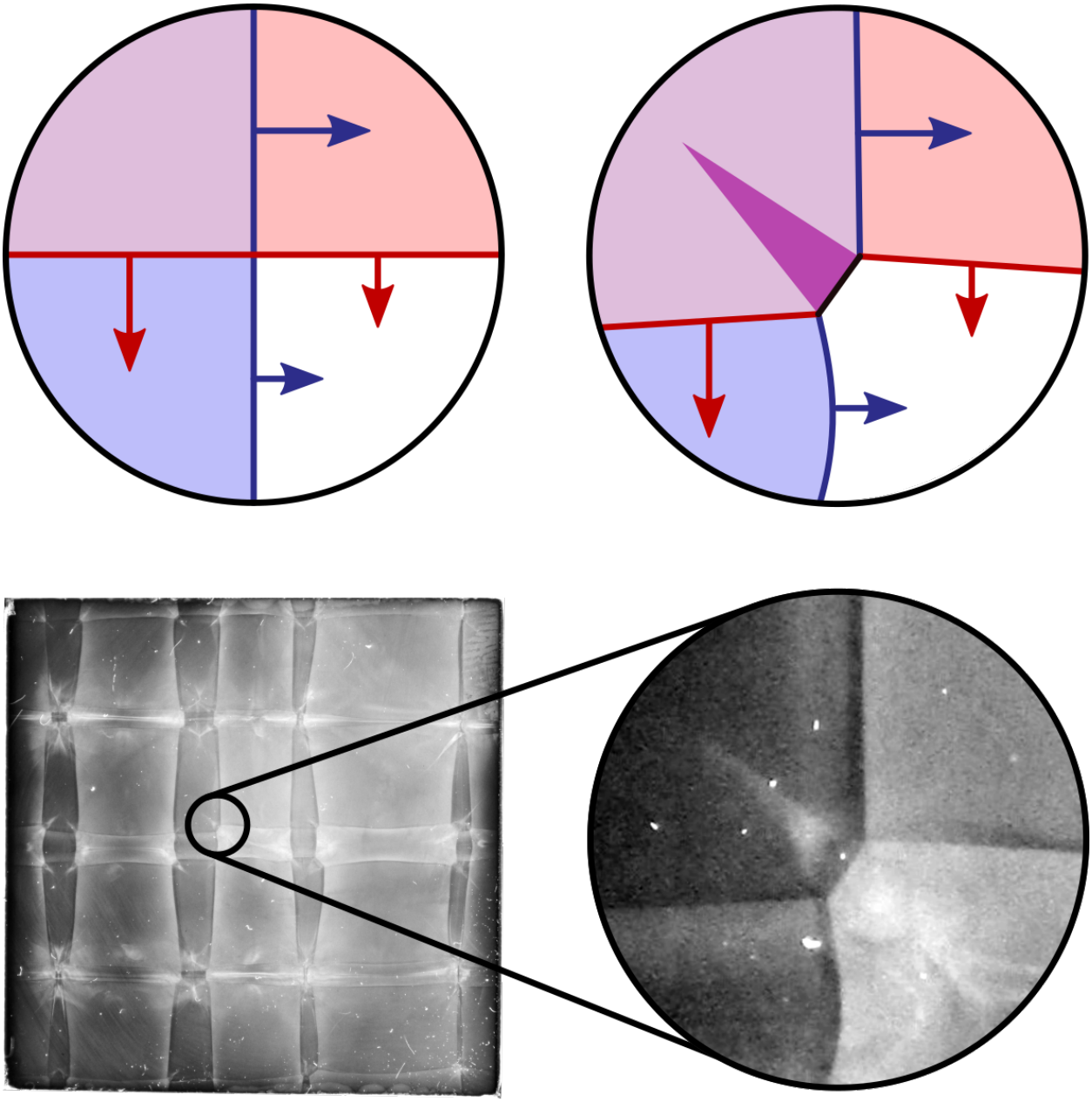

Figure 12: Blowup of crossing transverse waves

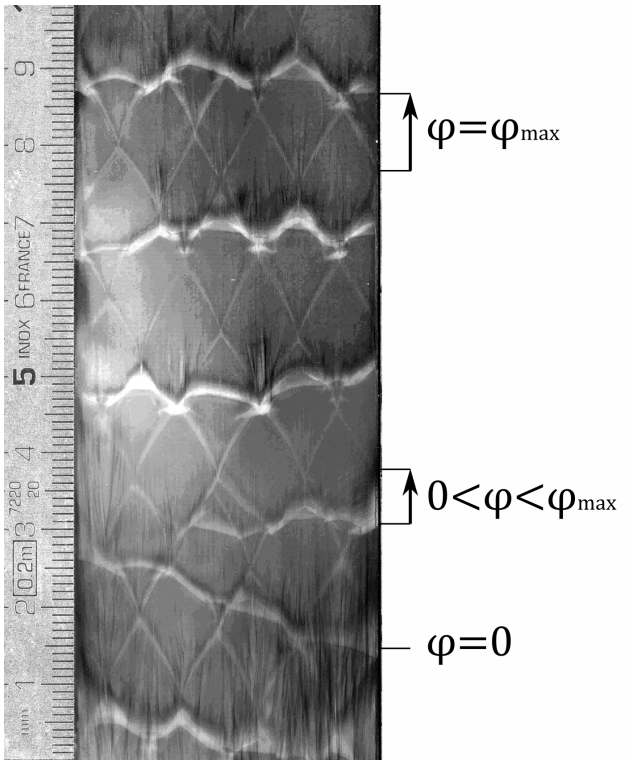

Figure 13: Example of phase shift φ varying from 0 to φ_{max} on a longitudinal soot recording for the $2\,H_2 + O_2 + 2\,Ar$ mixture at $p_0 = 15.0$ kPa.

4. Equivalent front-view tessellation for many cells

The analysis of the experimental front-view recordings indicate that the influence of the cross-section shape of the tube on the cellular patterns decreases with increasing initial pressure p_0 (Subsect. 3.1). Above a limiting value of p_0, all front-view patterns show a similar-looking irregularity regardless of this shape, that is, without evident periodicity in the relative positions of the cell edges. Paradoxically, the longitudinal recordings show the classical diamond-shaped regular arrangements typical of the considered mixture, both below and above the limit of influence of the cross-section shape. Therefore, longitudinal recordings alone cannot characterize the cellular structure. Determining average widths and patterns independent of the shape and area of the tube cross-section demands measurements with different cross-section shapes and increasing p_0 (Figure 7). Indeed, the average widths obtained from the longitudinal recordings converge with increasing p_0.

This subsection thus discusses the definition and the representativeness of an average cell width λ using front-view recordings obtained in conditions presumably independent of the cross-sections, that is, with many irregular cells. By dimensional analysis this width should be of the form $j\sqrt{A_t/F}$ where A_t is the tube cross-section, F the number of cells on the front-view recording and j an $O(1)$ geometrical factor that depends on some representative cell pattern independent of the tube. The premise here is that several front-view recordings obtained with the same composition and the same large enough p_0 show the same statistical distributions of different cell patterns, such as triangle, square, pentagon, hexagon, etc. Equivalently, the front-view distribution, at large F, of the same pattern, is statistically independent of the impact instant of cellular fronts generated in several experiments carried out in the same conditions. Elements from graph theory and tessellation, [72] can then be used to obtain an equivalence to this pattern distribution, and hence a representative cell width.

The cells on a front-view recording can thus be viewed as a set of faces that forms a planar graph governed by the Descartes-Euler-Poincaré relation

$$V - E + F = 2, \tag{2}$$

which constrains the numbers of faces F, edges E (the transverse waves plus the intersections of the cells with the tube wall(s)), and vertices V (the intersections of transverse waves with themselves plus those with the tube wall(s)). The right-hand side of relation (2) is 1 for a polygon. Formally, the number of faces F in (2) thus includes the outer (embedding) face, whose edges physically represent the tube walls. The conditions that each edge is common to exactly 2 faces and each vertex to at least 3 faces then give the assembly constraint

$$2E - 3V = k \geq 0, \tag{3}$$

where the integer k is the total number of edges supernumerary to 3 on a vertex, so $k = 0$ if all vertices are common to exactly 3 edges. Combining (2) and (3) yields the average edge number per face,

$$\frac{2E}{F} = 6\left(1 - \frac{2}{F}\right) - \frac{2k}{F}. \tag{4}$$

In this work, the blowup of the crossing locus of transverse waves suggests that any vertex can be common to only 3 edges (Section 3.2, Figure 8, Figure 12). All intersects are indeed Mach configurations with three transverse waves. Therefore, $k = 0$ here, so relation (4) for the average number of edges per face and its limit at large F reduce to

$$\frac{2E}{F} = 6\left(1 - \frac{2}{F}\right), \quad \lim_{F\to\infty} \frac{2E}{F} = 6. \tag{5}$$

A front-view recording with a large number of irregular cells is thus equivalent to a planar graph with the same number of hexagonal cells, that is, the hexagon is the representative pattern for cells considered as elements of a large set. The corresponding representative cell width can then be defined as the average of the inner and outer diameters of the regular hexagon, that is, of the distances between facing edges and facing vertices, respectively,

$$\lambda = \frac{6}{\pi}\int_0^{\frac{\pi}{6}} \frac{dx}{\cos x} \times d_i = \frac{3\ln(3)}{\pi}\, d_i \approx 1.049\, d_i, \tag{6}$$

where $d_i = \sqrt{2A_h/\sqrt{3}}$ and $A_h = A_t/F$ are the inner diameter and the area of the hexagon, and A_t is the cross-section area of the tube; hence,

$$\lambda = \frac{3\ln(3)}{\pi}\sqrt{\frac{2}{\sqrt{3}}\frac{A_t}{F}} \approx 1.127\sqrt{\frac{A_t}{F}}. \tag{7}$$

If one accepts two-wave transverse crossing, that is, four edges per vertex, such as those of front-view patterns approximated by rectangles and squares in a Q tube at low p_0 (Section 3.2), the number of edges supernumerary to 3 on a vertex, per face, k/F, is 1, not 0. Relation (4) and its limit at large F then reduce to

$$\frac{2E}{F} = 4 - \frac{6}{F}, \quad \lim_{F\to\infty} \frac{2E}{F} = 4. \tag{8}$$

Here, the representation of a large number of irregular cells is a planar graph with the same number of square cells whose average width is

$$\lambda = \frac{4}{\pi}\int_0^{\frac{\pi}{4}} \frac{dx}{\cos x} \times d_i \approx 1.122\, d_i = 1.122\sqrt{\frac{A_t}{F}}, \tag{9}$$

where $d_i = \sqrt{A_q}$ and $A_q = A_t/F$ are the distance between facing edges (a) and the area of the square cell, and A_t is the cross-section area (a^2) of the tube.

There are three observations. The first is that the average cell width for a large number of cells does not essentially depend on the actual representative cell pattern. A rough count from the recording at $p_0 = 70$ kPa in the 40×40-mm^2 Q tube (Fig. 6) gives $F \simeq 650$, and relation (7) for $F = 600$, 650 and 700 then gives $\lambda = 1.84$, 1.77 and 1.70 mm, respectively.

These averages agree with our measurements (Fig. 7) and those of Barthel [67] and Strehlow [29] (also in [68]) although these authors do not indicate the dimensions of their tubes.

The second observation is that the sensitivity $\Delta F/2F$ to the front-view cell number is relatively low. The cell count can indeed be difficult, depending on the quality of the front-view recordings. Relation (7) gives a relevant lower bound for measured cell widths, that is, measured values larger than the average value (7) indicate the persisting influence of the cross-section shape and area.

The third observation is that relations (7) and (9) define intrinsic, minimum, uncertainties on the cell width $\Delta\lambda/\lambda$ as the relative differences of the edge-to-edge and vertex-to-vertex distances, that is, $1-\sqrt{3}/2 \simeq 13.4\%$ for the hexagonal cell and $1-1/\sqrt{2} \simeq 29.3\%$ for the square cell. Thus, the uncertainty is about twice smaller if the representative cell is a hexagon. However, both uncertainties are large, which questions whether a single length can characterize front-view detonation cells.

A step forward could result from the comparison in Figure 14) suggesting that a front-view of detonation cells (left) closely resembles a Voronoi tessellation (right).A Voronoi element is the set of the closest points to a single source point in that set. Its boundaries would represent the transverse waves of the detonation front, and its source point the re-ignition locus from which these waves originated. The counting of the non-truncated Voronoi elements in Figure 14) yields $F = 73$ faces composed of 0 triangles, 12 rectangles, 21 pen-tagons, 25 hexagons, 13 heptagons, and 2 octagons. The majority, 63%, are pentagons or hexagons, i.e., with 5 or 6 edges, which is consistent with the upper bound 6 indicated by the relation (5). Here indeed, $2E/F = 5.62$, which is close to $6(1-1/F) = 5.92$. This slight

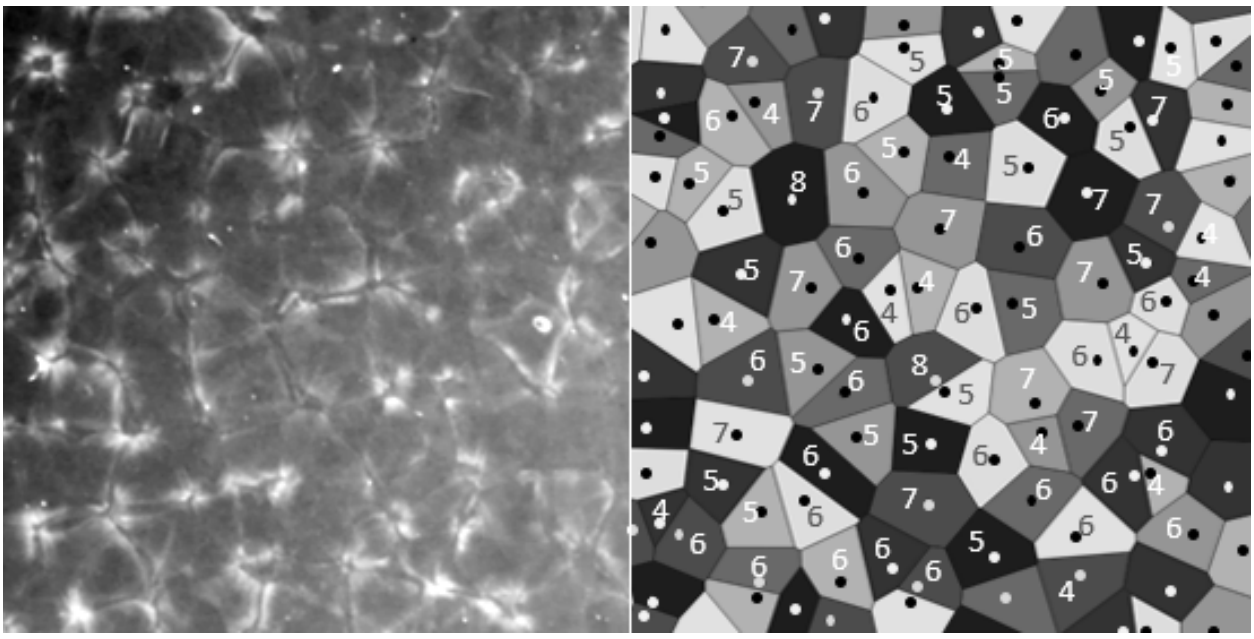

Figure 14: Front-view recording in the Q tube extracted from Figure 6(left) and Voronoi tessellation with randomly-distributed point sources (right).

deviation may result from the number of faces $F = 73$ not being large enough. Statistics from a tenth of other similarly-generated tessellations give about the same distribution and the same deviation, with very few or zero triangles and octagons, and only once a nonagon. In this example, the boundaries of the tessellation elements are not the contours of the detonation cells on the experimental extract because these are not defined well enough for a valuable automatic detection. Instead, we generated the Voronoi tessellation from a random distribution of sources, the number of which we chose so that the elements had similar dimensions to the experimental extract. This tessellation technique thus represents a mathematical model for the front-view of a cellular detonation suited to alternate modelling such as a cellular automaton. As its stands, however, a supplementation with a physical criterion is necessary to predict the number of source points per unit front surface.

5. Discussion and conclusions

The results above aim at providing an experimental basis for revisiting the notions of regularity and characteristic width for detonation cells. We implemented the soot-plate technique to record front-view and longitudinal traces of the cellular structure of the detonation front in the mixture $2\,H_2 + O_2 + 2\,Ar$ at the initial temperature $T_0 = 294$ K and the initial pressure p_0 varying from 15 kPa to 100 kPa (Sect. 2). This mixture is termed stable because its detonation cells in a tube with a square or a rectangular cross-section show regular diamond-shaped patterns on longitudinal recordings and, for low-enough p_0, alternate square and rectangular patterns on front-view recordings. In this study, we analyzed its cellular dynamics in detonation tubes whose cross-sections have the same surface area but different shapes, namely square, triangular and round (Sect. 3).

This work addressed only the case of the mixture $2\,H_2 + O_2 + 2\,Ar$, for which exists conditions on geometry and chemical kinetics for observing regularity. Therefore, a similar investigation is necessary to characterize the cellular dynamics of irregular mixtures such as heavy fuels diluted with nitrogen, depending on the cross-section shape of the tubes.

The distinction between regular and irregular cells or between stable and unstable mixtures relies essentially on longitudinal recordings in square cross-section tubes. However, we found that longitudinal and front-view recordings do not define the same regularity. Whereas the cell patterns on the longitudinal recordings are regular for all considered p_0 and cross-section shapes, those on the front-view recordings are irregular except for the square shape and low-enough p_0 (Subsect. 3.1). Therefore, the cellular dynamics at the walls of a tube is not representative of that on the whole detonation front, and longitudinal soot traces alone are not sufficient for describing the cellular structure. Our experimental results indicate that a large number of cells is necessary for characterizing cells by a single length. At large enough p_0, all front-view recordings show irregular cells with the same average width, that is, independent of the cross-section shape and area. The lower limits of p_0 above which cells are irregular and have the same width regardless of the cross-section appear to be the same in our conditions. However, more recordings are necessary to remove uncertainty.

We presented geometrical elements from graph theory suggesting that a tessellation of

hexagons can model a large set of irregular cells on a front-view recording (Sect. 4). This defines a cell average width λ and its intrinsic minimum relative error $\Delta\lambda/\lambda \simeq 13.4\%$. Our cell count on the front-view recording at the estimated limiting p_0 for irregularity, combined with the relation for λ from graph theory, results in the same value as interpolated from measurements on longitudinal recordings. This supports that cells are irregular for this p_0.

The large value $\mathcal{O}(0.1)$ of the intrinsic minimum relative error emphasizes the difficulty for numerical simulation to represent a detonation front with many cells, essentially the right balance between numerical accuracy and physical representativeness of the chemical kinetics. For example, considering the simple global Arrhenius rate of chemical progress and denoting E_a the activation energy, R the universal gas constant and T_H the shock temperature, we have $\lambda \propto \exp(E_a/RT_H)$ in the limit of large reduced activation energy E_a/RT_H, hence

$$\frac{\Delta E_a}{E_a} = \frac{RT_H}{E_a}\frac{\Delta\lambda}{\lambda}. \tag{10}$$

The typical values $T_H = 1500$ K and $E_a = 20$ kcal/mole, with molecular mass $M = 20\times10^{-3}$ kg/mole, $R = 8.314$ J/mole/K, and $\Delta\lambda/\lambda \approx 0.1$ then gives $\Delta E_a/E_a \approx 0.3\%$. This small number implies that values of E_a can always be found for satisfactory restitution of a single characteristic length such as λ, although this Arrhenius rate cannot often represent the actual kinetics. The physical interpretation is that both a detailed scheme of chemical kinetics and more advanced conceptual tools than a single length are necessary for characterizing detonation cells.

Our analysis also indicates a continuous variation of the phase shift of the multi-cellular rectangular mode in square tubes at low or moderate initial pressures (Subsect. 3.2). We suggested that detonation propagation in this case is also subjected to long-wavelength and low-amplitude instabilities - compared to the cell dynamics - with characteristic times at least the effective reaction time. These include an intrinsic instability of the rectangular mode growing with increasing cell number, that is, p_0, small defects at walls and persisting asymmetry of the wave front after ignition.

The simulation of cellular detonations should thus also include initial and boundary conditions with stochastic distributions of defects representative of actual devices. Today, this simulation relies essentially on Euler's equations for compressible reactive fluids. However, the uncertainties in the numerical technique, chemical kinetics, equations of state, multi-physics of interface phenomena, and hence the still very long computation times for three-dimensional waves do not make the physical interpretation of the computations less uneasy and time-consuming than that of the experiments.

Simplified partial differential equations with the same mathematical hyperbolic structure as Euler's, such as Burger's with a non-viscous source term, are modelling substitutes helpful to understand detonation instabilities and structures [73–76]. Combining simulation and modelling with applied mathematics tools on pattern generation and arrangements, such as information entropy and Voronoi tessellations [72], could bring detonation cell analysis closer to the mathematical corpus of dynamical systems and help to better characterize distributions with several cell patterns (Sect. 4).

Acknowledgements

This work was supported by the Ministry of Higher Education, Research and Innovation (France)

References

[1] Y. N. Denisov, Y. K. Troshin, Pulsating and spinning detonation of gaseous mixtures in tubes, Dokl. Akad. Nauk SSSR 125 (1959) 110–113.

[2] C. Campbell, D. W. Woodhead, The ignition of gases by an explosion-wave. Part I. Carbon monoxide and hydrogen mixtures, J. Chem. Soc. 129 (1926) 3010–3021. doi:10.1039/JR9262903010.

[3] P. Clavin, G. Searby, Combustion Waves and Fronts in Flows: Flames, Shocks, Detonations, Ablation Fronts and Explosion of Stars, Cambridge University Press, 2016. doi:10.1017/CBO9781316162453.

[4] A. Higgins, Steady one-dimensional detonations, in: F. Zhang (Ed.), Shock Waves Science and Technology Library, Vol. 6, Springer, Berlin, Heidelberg, 2012, pp. 33–105. doi:10.1007/978-3-642-22967-1_2.

[5] H. D. Ng, Detonation instability, in: F. Zhang (Ed.), Shock Waves Science and Technology Library, Vol. 6, Springer, Berlin, Heidelberg, 2012, pp. 107–212. doi:10.1007/978-3-642-22967-1_3.

[6] A. A. Vasil'ev, Dynamic parameters of detonation, in: F. Zhang (Ed.), Shock Waves Science and Technology Library, Vol. 6, Springer, Berlin, Heidelberg, 2012, pp. 213–279. doi:10.1007/978-3-642-22967-1_4.

[7] D. Desbordes, H.-N. Presles, Multi-scaled cellular detonation, in: F. Zhang (Ed.), Shock Waves Science and Technology Library, Vol. 6, Springer, Berlin, Heidelberg, 2012, pp. 281–338. doi:10.1007/978-3-642-22967-1_5.

[8] F. A. Bykovskii, Continuous spin detonations, J. Propuls. Power 22 (2006) 1204–1216. doi:10.2514/1.17656.

[9] J. E. Shepherd, J. Kasahara, Analytical models for the thrust of a rotating detonation engine, Tech. Rep. FM2017.001, Explosion Dynamics Laboratory, California Institute of Technology Report (2017). doi:10.7907/DNVT-PY80.

[10] P. Wolanski, Research on detonative propulsion, Lukasiewicz Research Network - Institute of Aviation, ISBN: 978-83-63539-45-0, 2021.

[11] A. A. Vasil'ev, Cell size as the main geometric parameter of a multifront detonation wave, J. Propuls. Power 22 (2006) 1245–1260. doi:10.2514/1.20348.

[12] R. Soloukhin, Nonstationary phenomena in gaseous detonation, Symp. (Int.) Combust. 12 (1) (1969) 799–807. doi:10.1016/S0082-0784(69)80461-3.

[13] J. H. S. Lee, M. I. Radulescu, On the hydrodynamic thickness of cellular detonations, Combust. Explos. Shock Waves 41 (6) (2005) 745–765. doi:10.1007/s10573-005-0084-1.

[14] M. I. Radulescu, G. J. Sharpe, C. K. Law, J. H. S. Lee, The hydrodynamic structure of unstable cellular detonations, J. of Fluid Mech. 580 (2007) 31–81. doi:10.1017/S0022112007005046.

[15] S. Boulal, P. Vidal, R. Zitoun, T. Matsumoto, A. Matsuo, Experimental investigation on detonation dynamics through a reactivity sink, Combust. Flame 196 (2018) 11–25. doi:10.1016/j.combustflame.2018.05.017.

[16] P. V. Tiggelen, J. Libouton, Evolution des variables chimiques et physiques à l'intérieur d'une maille de détonation, Ann. Phys. Fr. 14 (1989) 649 – 660. doi:10.1051/anphys:01989001406064900.

[17] G. J. Sharpe, J. J. Quirk, Nonlinear cellular dynamics of the idealized detonation model: Regular cells, Combust. Theor. Model. 12 (1) (2008) 1–21. doi:10.1080/13647830701335749.

[18] D. W. Stamps, S. R. Tieszen, The influence of initial pressure and temperature on hydrogen-air-diluent detonations, Combust. Flame 83 (3) (1991) 353–364. doi:10.1016/0010-2180(91)90082-M.

[19] Y. Auffret, D. Desbordes, H. Presles, Detonation structure of $C_2H_4 - O2 - Ar$ mixtures at elevated initial temperature, Shock Waves 9 (1999) 107–111. doi:10.1007/s001930050145.

[20] Y. Auffret, D. Desbordes, H. Presles, Detonation structure and detonability of $C_2H_2 - O_2$ mixtures at elevated initial temperature, Shock Waves 11 (2001) 89–96. doi:10.1007/PL00004069.

[21] G. Ciccarelli, T. G. Ginsberg, J. L. Boccio, The influence of initial temperature on the detonability characteristics of hydrogen-air-steam mixtures, Combust. Sci. Technol. 128 (1-6) (1997) 181–196. doi:10.1080/00102209708935708.

[22] J. Shepherd, Chemical kinetics of hydrogen-air-diluent detonations, in: J.-C. Leyer, R. Soloukhin, J. Bowen (Eds.), Dynamics of Explosions, Vol. 106, Progress in Astronautics and Aeronautics Series, 1986, pp. 263–293. doi:10.2514/5.9781600865800.0263.0293.

[23] A. Gavrikov, A. Efimenko, S. Dorofeev, A model for detonation cell size prediction from chemical kinetics, Combust. Flame 120 (1) (2000) 19–33. doi:10.1016/S0010-2180(99)00076-0.

[24] J. Shepherd, I. Moen, S. Murray, P. Thibault, Analyses of the cellular structure of detonations, Symp. (Int.) Combust. 21 (1) (1988) 1649–1658. doi:10.1016/S0082-0784(88)80398-9.

[25] H. Zhao, J. H. Lee, J. Lee, Y. Zhang, Quantitative comparison of cellular patterns of stable and unstable mixtures, Shock Waves 26 (10) (2016) 621–633. doi:10.1007/s00193-016-0673-9.

[26] Y. Zhang, L. Zhou, H. Meng, T. Honghui, Reconstructing cellular surface of gaseous detonation based on artificial neural network and proper orthogonal decomposition, Combust. Flame 212 (2020) 156–164. doi:10.1016/j.combustflame.2019.10.031.

[27] V. I. Manzhalei, V. V. Mitrofanov, V. A. Subbotin, Measurement of inhomogeneities of a detonation front in gas mixtures at elevated pressures, Combust. Explos. Shock Waves 10 (1974) 89–95. doi:10.1007/BF01463793.

[28] R. Strehlow, R. Liaugminas, R. Watson, J. Eyman, Transverse wave structure in detonations, Symp. (Int.) on Combust. 11 (1) (1967) 683–692. doi:10.1016/S0082-0784(67)80194-2.

[29] R. A. Strehlow, C. D. Engel, Transverse Waves in Detonations: II. Structure and Spacing in H_2—O_2, C_2H_2—O_2, C_2H_4—O_2, and CH_4—O_2 Systems, AIAA J. 7 (8) (1969) 492–496.

[30] V. I. Manzhalei, V. A. Subbotin, Stability of an overcompressed gas detonation, Combust. Explos. Shock Waves 12 (1976) 819–825. doi:10.1007/BF00740759.

[31] V. I. Manzhalei, Fine structure of the leading front of a gas detonation, Combust. Explos. Shock Waves 13 (1977) 402–404. doi:10.1007/BF00740325.

[32] I. O. Moen, G. O. Thomas, D. Bjerketvedt, P. A. Thibault, Influence of Cellular Regularity on the Behavior of Gaseous Detonations, Vol. 104, Progress in Astronautics and Aeronautics, 1986, Ch. III. Detonation Structure and Limit Propagation, pp. 220–243. doi:10.2514/5.9781600865800.0220.0243.

[33] C. Paillard, G. Dupré, H. A. Aiteh, S. Youssefi-Stitou, Influence de la cinétique chimique sur la structure des détonations : cas du bioxyde de chlore, in: Ann. Phys. Fr., EDP Sciences, 1989, pp. 641 – 648. doi:10.1051/anphys:01989001406064100.

[34] P. V. Tiggelen, J. Libouton, Evolution des variables chimiques et physiques à l'intérieur d'une maille de détonation, Ann. Phys. Fr. 14 (6) (1989) 649–660. doi:10.1051/anphys:01989001406064900.

[35] J. Austin, F. Pintgen, J. Shepherd, Reaction zones in highly unstable detonations, Proc. Combust. Inst. 30 (2) (2005) 1849–1857. doi:10.1016/j.proci.2004.08.157.

[36] S. I. Jackson, M. Short, The influence of the cellular instability on lead shock evolution in weakly unstable detonation, Combust. Flame 160 (10) (2013) 2260–2274. doi:10.1016/j.combustflame.2013.04.028.

[37] M. Short, G. J. Sharpe, Pulsating instability of detonations with a two-step chain-branching reaction model: theory and numerics, Combust. Theor. Model. 7 (2) (2003) 401–416. doi:10.1088/1364-7830/7/2/311.

[38] M. Radulescu, G. Sharpe, D. Bradley, A universal parameter quantifying explosion hazards, detonability and hot spot formation: χ number, in: D. Bradley, G. Makhviladze, V. Molkov, P. Sunderland, F. Tamanini (Eds.), Proceedings of the 7^{th} International Seminar on Fire and Explosion, Hazards, Research Publishing, 2013, pp. 617–626. doi:10.3850/978-981-07-5936-0_10-01.

[39] M. Hanana, M. H. Lefebvre, P. J. Van Tiggelen, On rectangular and diagonal three-dimensional structures of detonation waves, in: G. Roy, S. Frolov, K. Kailasanath, N. Smirnov (Eds.), Gaseous and Heterogeneous Detonations: Science to Applications, ENAS Publishers, 1998, pp. 121–129.

[40] N. Manson, Sur la structure des ondes explosives dites hélicoidales dans les mélanges gazeux, C. R. Hebd. Scéances Acad. Sci. 222 (1946) 46–50.

[41] J. A. Fay, A mechanical theory of spinning detonation, J. Chem. Phys. 20 (6) (1952) 942–950. doi:10.1063/1.1700655.

[42] J. Dove, H. Wagner, A photographic investigation of the mechanism of spinning detonation, Symp. (Int.) on Combust. 8 (1) (1961) 589–600. doi:10.1016/S0082-0784(06)80550-3.

[43] G. L. Schott, Observations of the structure of spinning detonation, Phys. Fluids 8 (5) (1965) 850–865. doi:10.1063/1.1761328.

[44] A. Macpherson, The three-dimensional wave system of spinning detonation, Symp. (Int.) Combust. 12 (1) (1969) 839–850. doi:10.1016/S0082-0784(69)80465-0.

[45] B. Voitsekhovskii, V. Mitrofanov, M. Topchian, Investigation of the structure of detonation waves in gases, Symp. (Int.) Combust. 12 (1) (1969) 829–837. doi:10.1016/S0082-0784(69)80464-9.

[46] R. A. Strehlow, Multi-dimensional detonation wave structure, Astronautica Acta. 15 (5-6) (1970) 345–357.

[47] M. Hanana, M. H. Lefebvre, P. J. Van Tiggelen, Pressure profiles in detonation cells with rectangular and diagonal structures, Shock Waves 11 (2001) 77–88. doi:10.1007/PL00004068.

[48] R. A. Strehlow, Gas phase detonations: Recent developments, Combust. Flame 12 (2) (1968) 81–101. doi:10.1016/0010-2180(68)90083-7.

[49] D. N. Williams, L. Bauwens, E. S. Oran, Detailed structure and propagation of three-dimensional detonations, Symposium (Int.) on Combustion 26 (2) (1996) 2991–2998. doi:10.1016/S0082-0784(96)80142-1.

[50] V. Deledicque, M. V. Papalexandris, Computational study of three-dimensional gaseous detonation structures, Combust. Flame 144 (4) (2006) 821–837. doi:10.1016/j.combustflame.2005.09.009.

[51] H.-S. Dou, H. M. Tsai, B. C. Khoo, J. Qiu, Simulations of detonation wave propagation in rectangular ducts using a three-dimensional WENO scheme, Combust. Flame 154 (4) (2008) 644–659. doi:10.1016/j.combustflame.2008.06.013.

[52] N. Tsuboi, S. Katoh, A. K. Hayashi, Three-dimensional numerical simulation for hydrogen/air detonation: Rectangular and diagonal structures, Proc. Combust. Inst. 29 (2002) 2783–2788. doi:10.1016/S1540-7489(02)80339-X.

[53] K. Eto, N. Tsuboi, A. K. Hayashi, Numerical study on three-dimensional c-j detonation waves: detailed propagating mechanism and existence of oh radical, Proc. Combust. Inst. 30 (2) (2005) 1907–1913. doi:10.1016/j.proci.2004.08.169.

[54] R. Deiterding, Numerical structure analysis of regular hydrogen-oxygen detonations, Proc. of Fall 2003 Meeting of Western States Section of The Combustion Institute Fall. URL https://resolver.caltech.edu/CaltechCACR:2003.210

[55] C. Wang, C.-W. Shu, W. Han, J. Ning, High resolution WENO simulation of 3D detonation waves, Combust. Flame 160 (2) (2013) 447–462. doi:10.1016/j.combustflame.2012.10.002.

[56] S. Borisov, A. Kudryavtsev, Investigation of cellular detonation structure formation via linear stability theory and 2D and 3D numerical simulations, in: Proceedings of the XXV Conference on High-Energy Processes in Condensed Matter, Vol. 1893, AIP Conf. Proc., 2017, pp. 1–11. doi:10.1063/1.5007500.

[57] S. Taileb, M. Reynaud, A. Chinnayya, F. Virot, P. Bauer, Numerical study of 3d gaseous detonations in a square channel., Aerotec. Missili Spaz. 97 (2018) 96–102. doi:10.1007/BF03405804.

[58] R. Takai, K. Yoneda, T. Hikita, Study of detonation wave structure, Symp. (Int.) Combust. 15 (1) (1975) 69–78. doi:10.1016/S0082-0784(75)80285-2.

[59] H. Presles, D. Desbordes, P. Bauer, An optical method for the study of the detonation front structure in gaseous explosive mixtures, Combust. Flame 70 (2) (1987) 207–213. doi:10.1016/0010-2180(87)90079-4.

[60] B. Voitsekhovskii, V. Mitrofanov, M. Topchian, Trad: The structure of the detonation front in gases, SO AN SSSR.

[61] K. I. Shchelkin, Y. K. Troshin, Gasdynamics of combustion, Tech. Rep. NASA-TT-F-231, National Aeronautics and Space Administration (1964).

[62] J. A. Fay, Gas pase detonations: Recent developments, Phys. Fluids 2 (3) (1959) 283–289. doi:10.1063/1.1705924.

[63] Y. Gao, B. Zhang, H. D. Ng, J. H. Lee, An experimental investigation of detonation limits in hydrogen–oxygen–argon mixtures, Int. J. of Hydrogen Energy 41 (14) (2016) 6076–6083. doi:10.1016/j.ijhydene.2016.02.130.

[64] W. W. Wood, J. G. Kirkwood, Diameter effect in condensed explosives. the relation between velocity and radius of curvature of the detonation wave, J. Chem. Phys. 22 (1954) 1920–1924. doi:10.1063/1.1739940.

[65] J. B. Bdzil, Steady-state two-dimensional detonation, J. Fluid Mech. 108 (1981) 195–226. doi:10.1017/S0022112081002085.

[66] M. Chiquete, M. Short, Characteristic path analysis of confinement influence on steady two-dimensional detonation propagation, J. Fluid Mech. 863 (2019) 789–816. doi:10.1017/jfm.2018.995.

[67] H. Barthel, Predicted spacings in hydrogen-oxygen-argon detonations, Phys. Fluids 17 (1974) 1547–1553. doi:10.1063/1.1694932.

[68] M. Kaneshige, J. Shepherd, Detonation database, California Institute of Technology; Online available; accessed march 2022 (2002).
URL https://shepherd.caltech.edu/detn_db/html/H2-Ox4.html

[69] J. H. S. Lee, The Detonation Phenomenon, Cambridge University Press, 2008, Ch. 6, p. 147–203. doi:10.1017/CBO9780511754708.007.

[70] R. K. Kumar, W. A. Dewit, Detonation cell widths in hydrogen/oxygen/diluent mixtures at low initial pressures, J. Energy Resour. Technol. 117 (1) (1995) 13–17. doi:10.1115/1.2835313.

[71] R. K. Kumar, Detonation cell widths in hydrogen/oxygen/diluent mixtures at low initial pressures, Combust. Flame 80 (1990) 157–169. doi:10.1016/0010-2180(90)90124-A.

[72] F. Aurenhammer, R. Klein, Voronoi diagrams, in: J.-R. Sack, J. Urrutia (Eds.), Handbook of Computational Geometry, North-Holland, Amsterdam, 2000, pp. 204–209. doi:10.1016/B978-044482537-7/50006-1.

[73] W. Fickett, Detonation in miniature, Am. J. Phys. 47 (1979) 1050–1059. doi:10.1119/1.11973.

[74] A. R. Kasimov, L. M. Faria, R. R. Rosales, Model for shock wave chaos, Phys. Rev. Lett. 110 (2013) 104–109. doi:10.1103/PhysRevLett.110.104104.

[75] A. R. Kasimov, Detonation analogs revisited, Proc. 25^{th} Int. Coll. Dynamics Explosion Reactive Systems (2015) paper 312.

[76] S. Lau-Chapdelaine, M. Radulescu, Detonation model using Burgers equation and a pulsed reaction, Proc. 27^{th} Int. Coll. Dynamics Explosion Reactive Systems (2019) paper 315.